A&A, 690, L16 (2024)
https://doi.org/10.1051/0004-6361/202451445

Astronomy & Astrophysics

LETTER TO THE EDITOR

A photo-*z* cautionary tale: Redshift confirmation of COSBO-7 at *z* = 2.625

Shuowen Jin[1,2,⋆,⋆⋆], Nikolaj B. Sillassen[1,2], Jacqueline Hodge[3], Georgios E. Magdis[1,2,4], Francesca Rizzo[5,1], Caitlin Casey[6,1], Anton M. Koekemoer[7], Francesco Valentino[8], Vasily Kokorev[6], Benjamin Magnelli[9], Raphael Gobat[10], Steven Gillman[1,2], Maximilien Franco[6], Andreas Faisst[11], Jeyhan Kartaltepe[12], Eva Schinnerer[13], Sune Toft[1,4], Hiddo S. B. Algera[14,15], Santosh Harish[10], Minju Lee[1,2], Daizhong Liu[16], Marko Shuntov[1,4], Margherita Talia[17,18], and Aswin Vijayan[1,2]

(Affiliations can be found after the references)

Received 10 July 2024 / Accepted 1 October 2024

ABSTRACT

Photometric redshifts are widely used in studies of dusty star-forming galaxies (DSFGs), but catastrophic photo-z failure can undermine all redshift-dependent results. Here we report the spectroscopic redshift confirmation of COSBO-7, a strongly lensed DSFG in the COSMOS-PRIMER field. Recently, a photometric redshift solution of $z \gtrsim 7.0$ was reported for COSBO-7 based on ten bands of *James Webb* Space Telescope (JWST) NIRCam and MIRI imaging data. This z value was favored by four independent spectral energy distribution (SED) fitting codes, and the result provided an appealing candidate for the most distant massive DSFG known to date. This photo-z solution was also supported by a single line detection in Atacama Large Millimeter Array (ALMA) Band 3 consistent with CO(7–6) at $z = 7.46$. However, our new ALMA observations robustly detect two lines in Band 6 identified as CO(7–6) and [CI](2–1) at $z_{\rm spec} = 2.625$, and thus the Band 3 line as CO(3–2). These three robust line detections decidedly place COSBO-7 at $z = 2.625$, refuting the photo-z solution. We derive physical parameters by fitting near-infrared(NIR)-to-millimeter(mm) photometry and lens modeling, revealing that COSBO-7 is a main sequence galaxy. We examine possible reasons for this photo-z failure and attribute it to (1) the likely underestimation of photometric uncertainties at 0.9 μm and 1.15 μm; and (2) the lack of photometry at wavelengths beyond 20 μm. Notably, we recover a bona fide $z_{\rm phot} \sim 2.3$ by including the existing MIPS 24 μm photometry, demonstrating the critical importance of mid-infrared (MIR) data in bolstering photo-z measurements. This work highlights a common challenge in modeling the SEDs of DSFGs, and provides a cautionary tale regarding the reliability of photometric redshifts as well as pseudo-spectroscopic redshifts based on single line detection.

Key words. galaxies: distances and redshifts – galaxies: high-redshift – galaxies: ISM – galaxies: individual: COSBO-7

1. Introduction

Redshift is one of the most important parameters of a galaxy, and determining the redshift of a galaxy is the first and most critical step in revealing its nature. To date, the most distant galaxies have been confirmed at $z \sim 14$ (Carniani et al. 2024) by spectroscopy from the *James Webb* Space Telescope (JWST). For dusty star-forming galaxies (DSFGs), given the severe dust attenuation and extreme faintness in optical and near-infrared (NIR) wavelengths (e.g., Wang et al. 2019; Smail et al. 2021), detecting molecular and neutral line features in millimeter (mm) and submillimeter(submm) wavelengths is a more efficient way of confirming their redshifts. Thanks to the advanced mm and submm interferometers, such as Atacama Large Millimeter Array (ALMA) and Northern Extended Millimeter Array (NOEMA), distant DSFGs have been spectroscopically confirmed at $z > 5$ and out to the epoch of reionization (EoR, $z \sim 7$; e.g., Walter et al. 2012; Vieira et al. 2010, 2013; Riechers et al. 2013, 2017; Strandet et al. 2017; Zavala et al. 2018; Marrone et al. 2018; Endsley et al. 2022; Fudamoto et al. 2021; Hygate et al. 2023; Rowland et al. 2024), proving these facilities to be a powerful "redshift machine" (Vieira et al. 2013; Neri et al. 2020; Chen et al. 2022; Cox et al. 2023).

However, performing spectroscopy on DSFGs remains observationally expensive, which limits the size and completeness of current spec-z samples. Alternatively, photometric redshifts, which are estimated by modeling spectral energy distributions (SEDs) with optical and NIR photometry (e.g., Arnouts et al. 1999; Ilbert et al. 2006; da Cunha et al. 2008; Brammer et al. 2008; Kriek et al. 2009; Carnall et al. 2018; Boquien et al. 2019), are widely used and dominate in literature studies of DSFGs (e.g., Boone et al. 2011; Wardlow et al. 2011; Simpson et al. 2014; Miettinen et al. 2015; Wang et al. 2019; Gómez-Guijarro et al. 2019; Dudzevičiūtė et al. 2020; Smail et al. 2021). In comparison to dust-free galaxies, constraining the redshifts of DSFGs is particularly challenging because of severe dust attenuation. Nowadays, the situation has been dramatically improved with the data from JWST. With its unprecedented sensitivity and long-wavelength coverage, photometric redshifts have been estimated out to $z > 10-16$ for dust-free galaxies (e.g., Naidu et al. 2022; Finkelstein et al. 2022; Harikane et al. 2023; Atek et al. 2023; Casey et al. 2024; Chakraborty et al. 2024) and $z \sim 8$ for DSFGs (e.g., Barrufet et al. 2023; Akins et al. 2023). Nevertheless, photometric redshifts can still fail catastrophically –that is, they can be catastrophically erroneous– for dust-free galaxies, even with multiband JWST photometry. For example, the galaxy CEERS-93316 was reported with a photometric redshift of $z \sim 16.4$ based on a SED fitting with seven bands of JWST NIRCam photometry (Donnan et al. 2023), but was eventually confirmed to be a

⋆ Corresponding author; shuji@dtu.dk
⋆⋆ Marie Curie Fellow.

$z = 4.9$ dusty galaxy based on JWST NIRSpec spectroscopy (Arrabal Haro et al. 2023), demonstrating that dusty starbursts can masquerade as ultrahigh-redshift galaxies (Zavala et al. 2023; Naidu et al. 2022). As the misidentification of photo-z can undermine all results that are dependent on redshift, it is vital to examine whether such photo-z failure can also happen for DSFGs preselected from mm and submm surveys.

Recently, a $z > 7$ DSFG candidate, COSBO-7, was reported by Ling et al. (2024) based on exquisite imaging data from JWST. Ling et al. (2024) performed extensive imaging fitting and SED analysis using the JWST NIRCam and MIRI data, and found that COSBO-7 is not detected in NIRCam/F090W but is well detected in nine bands from NIRCam/F115W to MIRI/F1800W. Using the photometry measured on the lens-subtracted images, these authors calculated photometric redshifts of $z_{\rm phot} = 6.9$–7.7, finding that four SED algorithms, namely `LePhare` (Ilbert et al. 2006), `EAZY` (Brammer et al. 2008), `Bagpipes` (Carnall et al. 2018), and `CIGALE` (Boquien et al. 2019) agree on a best-fit solution of $z \sim 7.0$. This makes COSBO-7 an appealing candidate for the most distant DSFG to date. Furthermore, Ling et al. (2024) reported a line detection at 95.4 GHz in ALMA archival data that would be consistent with CO(7–6) emission at $z = 7.46$, that is, at a redshift very close to the $z_{\rm phot}$ solution. Nevertheless, robust spectroscopic confirmation with multiple lines was still missing.

In this Letter, we report unambiguous spectroscopic redshift confirmation of COSBO-7 and discuss the implications of erroneous photometric redshift estimates and the lessons learned from this cautionary tale. We adopt a flat ΛCDM cosmology with $H_0 = 70$ km s^{-1} Mpc^{-1} and $\Omega_M = 0.27$, and a Chabrier initial mass function (Chabrier 2003).

2. Selection and data

2.1. Selection

COSBO-7 (Right Ascension (RA) = 10:00:23.97, Declination (Dec.) = +02:17:50.0) was originally discovered in a flux-limited IRAM/MAMBO-2 1.2 mm imaging survey by Bertoldi et al. (2007). It is one of the brightest submm sources in the COSMOS field, and is also detected in the AzTEC and SCUBA-2 surveys ($S_{1\,\rm mm} \sim 2$ mJy, $S_{850\,\mu\rm m} \sim 10$ mJy; Aretxaga et al. 2011; Geach et al. 2017; Simpson et al. 2019). COSBO-7 is not detected in deep HST images of the COSMOS-CANDELS field, indicating an extremely dust-obscured nature. A secure counterpart of COSBO-7 was first identified in radio wavelengths at VLA 1.4 GHz and 3 GHz (Schinnerer et al. 2010; Smolčić et al. 2017). COSBO-7 was identified as a lensing system by Jin et al. (2018), wherein a high-z submillimeter galaxy is lensed by a foreground elliptical galaxy at $z_{\rm spec} = 0.36$. COSBO-7 was observed with ALMA Band 7 in the project 2016.1.00463.S (PI: Y. Matsuda) and was cataloged by Simpson et al. (2020). Recently, COSBO-7 was observed with JWST/NIRCam and MIRI as part of the PRIMER survey (Dunlop et al. 2021). The MIRI image clearly reveals a lensing arc in the MIRI 7.7 μm band while a counter-image is found on the ALMA 870 μm map (Pearson et al. 2024), confirming the strong lensing nature of the system. Ling et al. (2024) performed an extensive photometric analysis of COSBO-7 by exploiting the JWST imaging data from NIRCam F090W to MIRI F1800W band after subtracting the foreground lens. These authors found that COSBO-7 remains undetected in F090W, but is well detected in nine bands from F115W to F1800W. With the JWST photometry, Ling et al. (2024) performed SED fitting using four SED codes that all converged to a photo-z solution of $z \gtrsim 7.0$.

2.2. ALMA

The first spectroscopic follow-up of COSBO-7 was carried out with ALMA Band 3 line scans in Cycle 9 (ID:2022.1.00863.S; PI: J. Hodge) as part of a redshift scan program investigating ten radio-selected, optically dark DSFGs. A strong line was detected at 95.4 GHz (Fig. 1, bottom-left); however the single line detection was insufficient to confirm the redshift of the source. Driven by the photometric redshift $z \gtrsim 7.0$ by Ling et al. (2024), it was reasonable to postulate that the 95.4 GHz line originates from CO(7–6) emission at $z = 7.458$. Further, the $z = 7.458$ solution was also supported by a multitude of indirect evidence: (1) a tentative line at 95.7 GHz, consistent with [CI](2-1) emission at $z = 7.458$; (2) F410M excess, indicative of [OIII]+Hβ emission at $z \sim 7.4$; (3) MIPS 24 μm excess that is consistent with a 3.3 μm polycyclic aromatic hydrocarbon (PAH) feature at $z = 7.458$; and (4) a well-fitted panchromatic SED from NIR to radio wavelengths. However, without a robust detection of a second line, the redshift of the source remained ambiguous. Consequently, we proposed 0.5 hr of ALMA Band 6 observations through DDT time, aiming to detect [CII]158 μm and decidedly determine the redshift of COSBO-7.

The DDT program (ID: 2023.A.00021.S; PI: S. Jin) was approved and the observation was executed on March 21 2024 in C-1 configuration. The frequency tuning covers 222.18–225.94 GHz for lines and 235.60–239.48 GHz for continuum. The on-source integration is 15 mins, and self-calibration was performed. This gives a rms sensitivity of 0.107 mJy/beam per 500 km s^{-1}, and a beam size of $1.43'' \times 1.14''$ with natural weighting.

The raw data of the ALMA programs mentioned above were reduced and calibrated using the standard ALMA CASA pipeline (McMullin et al. 2007). Following our established pipeline from Jin et al. (2019, 2022), we converted the calibrated measurement sets to `uvfits` format for further analysis in uv space with the GILDAS software. The 1D spectrum was extracted using the GILDAS `uvfit` routine on the uv tables at all frequencies, where we adopted a point-source model on the fixed position of the ALMA continuum peak. The continuum and line maps are cleaned using the GILDAS HOGBOM clean routine. Given that COSBO-7 is resolved in the ALMA data, we measured the continuum and integrated line fluxes on the clean images using an aperture of $r \sim 2.5''$, which maximizes the integrated S/Ns. We also measured the photometry in ALMA Band 4 (ID: 2021.1.00705.S; PI: O. Cooper), and adopted 870 μm photometry in the A3COSMOS catalog (Liu et al. 2019) measured from Band7 data (ID: 2016.1.00463.S, PI: Y. Matsuda). We list the line fluxes in Table 1 and continuum fluxes in Table A.1.

2.3. JWST

COSBO-7 was observed with JWST NIRCam and MIRI in ten bands: F090W, F115W, F150W, F200W, F277W, F356W, F410M, and F444W in NIR, and F770W and F1800W in mid-infrared (MIR). Ling et al. (2024) modeled the foreground lens using `Galfit` and measured the photometry on the lens-subtracted residual images. The lens is well modeled, and so the counter image of the arc is recovered in the residual map. The photometry was carefully measured on the PSF-matched and aperture-matched residual images, and therefore we directly adopt the photometry from Ling et al. (2024). As Ling et al. (2024) measured 2σ upper limits of F090W using two different

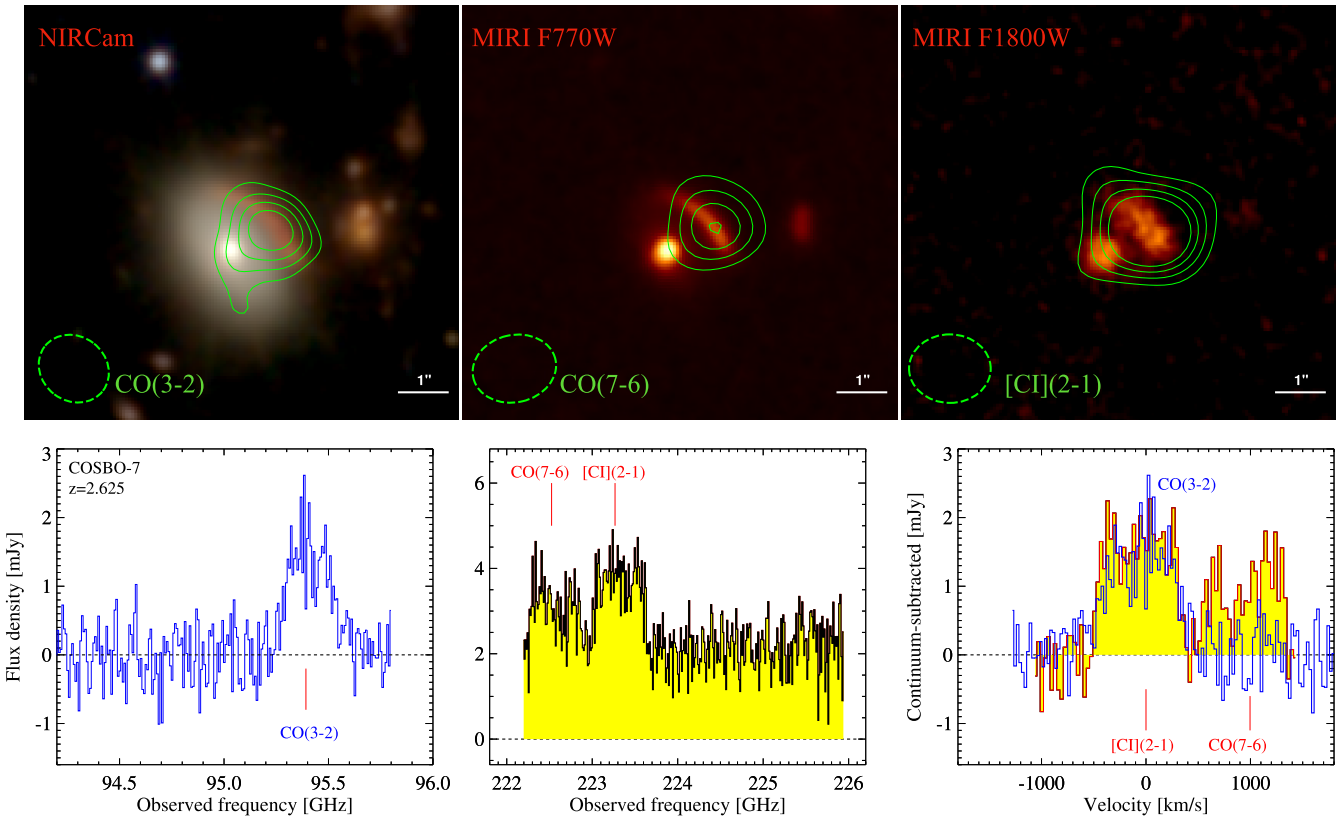

Fig. 1. JWST images and ALMA spectra of COSBO-7. *Top*: NIRCam color image (Blue: F090W+F115W+F150W; Green: F200W+F277W; Red: F356W+F410M+F444W), and MIRI images overlaid with contours of CO and [CI] emission. Contours are shown at 4, 6, 8, and 10σ levels. The beams are shown as dashed ellipses. *Bottom*: Left and middle panels show the CO(3–2) and CO(7–6)+[CI](2–1) spectra in observed frequencies. The right panel shows the continuum-subtracted spectra as a function of velocity.

apertures, we adopted the flux limit measured within the larger aperture, but use the 3σ limit in this work for reasons discussed in Sect. 4.1. For visualization and lensing modeling, we used the PRIMER mosaics produced by M. Franco and S. Harish from the COSMOS-Web team (Casey et al. 2023).

2.4. Ancillary data

The FIR and radio photometry of COSBO-7 were already measured in the COSMOS Super-deblended catalog (Jin et al. 2018). However, the Herschel photometry is noisy because too many priors were fitted within the Herschel beams; that is, it exhibits a high level of crowding. The ALMA data show that COSBO-7 is the only submm-emitting source within the ALMA Band 7 ($r < 8''$) and Band 3 primary beam ($r < 30''$), indicating negligible blending and no contributions from neighboring sources. Hence, we reran our "super-deblending" pipeline with improved priors on Herschel maps as done by Sillassen et al. (2024), assuming that COSBO-7 is the only source contributing to the Herschel fluxes. As listed in Table A.1, the newly measured Herschel photometry shows solid detection in the PACS 160 μm and the SPIRE bands (Fig. 2).

3. Results

3.1. Redshift confirmation

As shown in the bottom-middle panel of Fig. 1, the DDT program did not detect any line at the expected frequency of 224.7 GHz of [CII] at $z = 7.458$. Instead, and quite surprisingly, two lines are solidly detected at 222.52 GHz and 223.27 GHz with S/N= 11 and 23, respectively (Fig. 1). The two lines perfectly match the CO(7–6) and [CI](2–1) transitions at $z = 2.625$. Moreover, the 95.4 GHz line is also fitted at the exact frequency of $z = 2.625$ CO(3–2). Further, the line widths of the [CI] and CO lines are also consistent with a full width at zero intensity FWZI = 850 km s^{-1} (Fig. 1, bottom-right). Therefore, the three solid line detections unambiguously confirm the redshift of COSBO-7 to $z_{\rm spec} = 2.625$ instead of $z_{\rm phot} \gtrsim 7.0$.

3.2. Physical properties and lensing model

With the confirmed $z_{\rm spec} = 2.625$, we derive some physical parameters of COSBO-7 by SED fitting with multiwavelength photometry. As shown in Fig. 2, the SED is well fitted from NIR to radio wavelengths using `Stardust` (Kokorev et al. 2021). Specifically, the MIPS 24 μm excess is well fitted by strong PAH features at a rest-frame of 6−8 μm, while the MIR AGN contribution to the total IR luminosity is negligible (<2%). We report the best-fit parameters in Fig. 2 and Table 1. We note that the 3 mm continuum is not fitted well by `Stardust`, which suggests a steep β slope or optically thick dust in FIR (Jin et al. 2022). We thus performed FIR SED fitting with modified blackbody models using the `Mercurius` code (Witstok et al. 2022), accounting for both cases of optically thin and thick dust in FIR (Jin et al. 2022). As shown in Fig. A.1, the optically thick model performs slightly better than the thin ones, yielding a dust temperature of $T_{\rm dust} = 36.5 \pm 0.6$ K and a dust mass of $M_{\rm dust} = (2.9 \pm 0.3) \times 10^9\ M_\odot$. The dust temperature is consistent with the $T_{\rm dust} - z$ relation of main sequence galaxies by Schreiber et al. (2018).

Table 1. Physical properties of COSBO-7.

ID	COSBO-7
RA	10:00:23.97
Dec	+02:17:50.0
z	2.6250 ± 0.0007
μ	$3.6^{+2.0}_{-0.9}$
$I_{CO(3-2)}$ [Jy km s^{-1}]	1.93 ± 0.11
$I_{CO(7-6)}$ [Jy km s^{-1}]	0.88 ± 0.08
$I_{[CI](2-1)}$ [Jy km s^{-1}]	1.80 ± 0.08
A_V [mag]	1.95 ± 0.01
M_* [10^{11} M$_\odot$]	2.50 ± 0.23
SFR$_{IR}$ [M$_\odot$ yr^{-1}]	521^{+122}_{-45}
$M_{gas,[CI]}$ [10^{11}M$_\odot$]	5.04 ± 1.70
SFE [Gyr^{-1}]	1.03 ± 0.35
$T_{dust,thick}$ [K]	$36.5^{+0.6}_{-0.6}$
$M_{dust,thick}$ [10^9M$_\odot$]	$2.9^{+0.3}_{-0.3}$
$T_{dust,thin}$ [K]	$25.9^{+1.0}_{-0.9}$
$M_{dust,thin}$ [10^9M$_\odot$]	$5.3^{+0.9}_{-0.7}$

Notes. These parameters are not corrected for magnification μ.

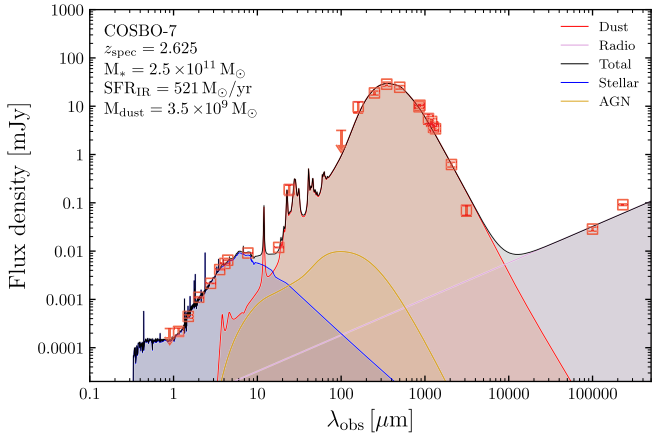

Fig. 2. Panchromatic SED of COSBO-7 fitted with `STARDUST` (Kokorev et al. 2021). The F090W upper limit is shown at the 3σ level. Radio photometry is not included in the fitting; we extrapolated a radio component using the IR luminosity and the IR–radio relation from Delvecchio et al. (2021). Parameters are not corrected for lensing magnification.

To constrain the magnification μ, we performed lens modeling of the F777W image by adopting the methodology from Vegetti & Koopmans (2009) and Rizzo et al. (2018). As shown in Fig. A.2, the lensing arc is well modeled with a magnification factor of $\mu = 3.6^{+2.0}_{-0.9}$. This magnification is consistent with the findings of Pearson et al. (2024), which are based on F777W data, but is slightly higher than the value estimated by Ling et al. (2024) from the F444W image.

We derive the molecular gas mass using [CI](2–1) and CO(3–2) as gas tracers: (1) Adopting a $R_{[CI]} = La'_{[CI](2-1)}/L'_{[CI](1-0)} = 0.3 \pm 0.1$ (Jiao et al. 2019) and assuming the excitation $T_{exc} = T_{dust,thick}$, we obtain a gas mass of $M_{gas,CI} = (5.04 \pm 1.70) \times 10^{11}\ M_\odot$ using the scaling relation from Valentino et al. (2018). (2) Assuming a CO line ratio of $r_{31} = 0.84 \pm 0.26$ from Riechers et al. (2020), we obtain a CO(1–0) luminosity of $L'_{CO(1-0)} = (7.7 \pm 2.4) \times 10^{11}$ K km s^{-1} pc^2, which gives a gas mass of $M_{gas,\alpha_{CO}=3.6} = (2.8 \pm 0.9) \times 10^{12}\ M_\odot$, or $M_{gas,\alpha_{CO}=0.4} = (3.1 \pm 1.0) \times 10^{11}\ M_\odot$. The CO-derived gas masses agree with $M_{gas,CI}$ within the uncertainty of α_{CO}. We adopted a conservative SFR = 521^{+122}_{-42} M$_\odot$ yr^{-1} comprising the outputs and uncertainties from both `Stardust` and `Mercurius`. As both r_{31} and α_{CO} are uncertain, we simply adopted $M_{gas,CI}$ and derived a median gas depletion time of $\tau \sim 1$ Gyr with a lower limit of $\tau > 326$ Myr. This indicates that COSBO-7 is a gas-rich galaxy with a star formation efficiency (SFE) typical of main sequence galaxies (Sargent et al. 2014; Magdis et al. 2012, 2017). Accounting for the lensing magnification, the stellar mass and SFR of COSBO-7 are consistent with the main sequence at $z \sim 2.6$ (Schreiber et al. 2017). This again suggests that COSBO-7 is a typical dusty star-forming galaxy at $z \sim 2.6$ (e.g., da Cunha et al. 2015).

4. Discussion

4.1. Possible causes of the catastrophic photo-z failure

The robust $z_{spec} = 2.625$ for COSBO-7 derived in this study indicates that the photo-$z \gtrsim 7.0$ is a catastrophic failure and highlights that caution should be exercised in studies of DSFGs that rely on photometric redshifts. Here we attempt to uncover the reasons behind the photo-z failure and provide suggestions as to how to see through similar "cosmic conspiracies".

Interestingly, we find that the redshift probability distribution function PDF(z) by Ling et al. (2024) indeed shows an insignificant peak at $z \sim 2.6$ from `EAZY` and `CIGALE` results. As already tested by Ling et al. (2024), the PDF(z) at $z \sim 2.6$ became dominant if adopting the limit of $z < 6$ with `EAZY`, `CIGALE`, and `Bagpipes`. On the other hand, Ling et al. (2024) performed SED fitting with two different F090W upper limits, one of which is the average 2σ depth of the image measured in a $r = 0.2''$ aperture, while the other is a 2σ limit measured within the aperture used for the arc. These authors found that, in either case, the best PDF(z) solution remains peaked at $z \sim 7.0$, and that adjusting the F090W upper limit with a large aperture does not appear to improve the photo-z outputs. We also tested with `EAZY` by adopting the F090W 3σ upper limit, and found the best-fit output remains $z \sim 7$–8, consistent with Ling et al. (2024). As shown in the left panel of Fig. 3, we tested fitting NIR-to-MIR SEDs at both $z = 2.625$ and $z = 7.458$, finding that the SED can be fitted at both redshifts, with a subtle difference in the χ^2 values between the two solutions. This indicates that the NIR-to-MIR photometry is fully degenerated between $z \sim 2.6$ and $z \sim 7.5$. Further, we test `Bagpipes` fitting without the F090W upper limit. Interestingly, we find that the PDF(z) peaks at $z \sim 2.3$ without a secondary solution at $z > 7$, as in the left panel of Fig. 3. This photo-z is close to the $z_{spec} = 2.625$, and consistent within a typical uncertainty of $\Delta z/(1+z) < 10\%$. This well-recovered photo-z suggests that the F090W flux limit by Ling et al. (2024) might be underestimated. We note that the F090W limit in Fig. 3 is a 3σ upper limit, which is well above the best-fit models of either $z = 2.625$ or $z = 7.458$, while Ling et al. (2024) adopted a stricter 2σ upper limit. This stringent upper limit likely forced the templates to interpret the data at $\lambda < 1$ μm as a Lyman break at $z \sim 7$, while excluding solutions at lower redshifts.

Given that the 24 μm flux density is about ten times higher than the F1800W one, we suspect that such an excess, boosted by PAH emission, might be useful to improve the photo-z quality. Therefore, we tested fitting the SED by including the MIPS 24 μm photometry $S_{24\mu m} = 188.4 \pm 45.9$ μJy measured by Jin et al. (2018), which was not used by Ling et al. (2024). Strikingly, this again yields a $z_{phot} = 2.3$ (Fig. 3, right), and the χ^2

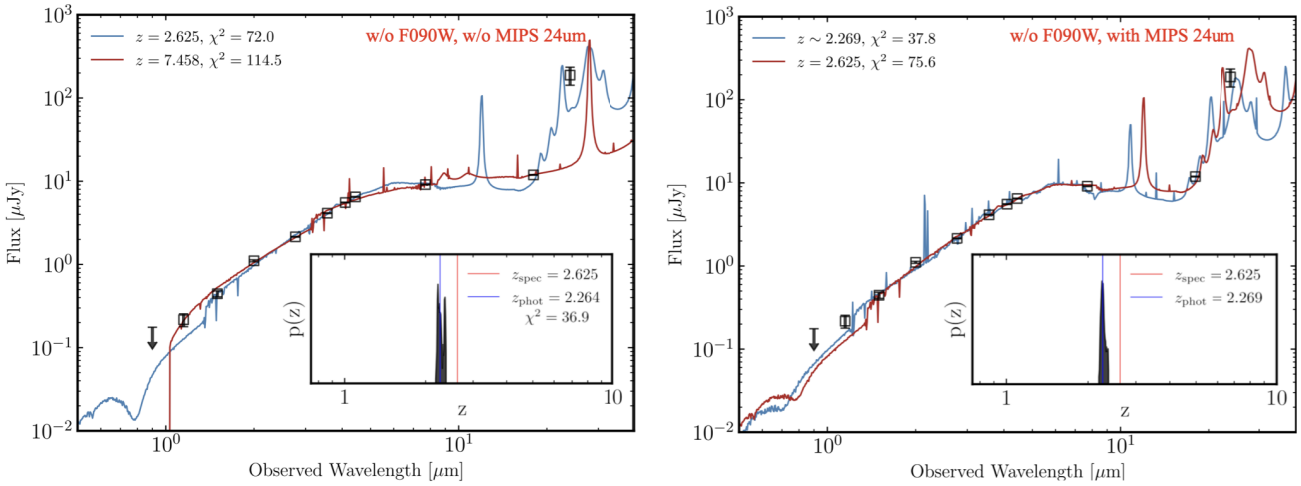

Fig. 3. NIR-to-MIR SED of COSBO-7 fitted with `Bagpipes`. *Left*: Fitting without the F090W upper limit and without 24 μm photometry with the PDF(z) shown in the subpanel. We also show the SEDs and χ^2 for both $z = 2.625$ and 7.458 cases. *Right*: Best fit with MIPS 24 μm photometry and without the F090W limit. We present the PDF(z) with z_{spec} in the subpanel.

is two times smaller than that of the fitting at fixed $z = 2.625$ without 24 μm. This is evident in the left panel of Fig. 3: it is difficult to fit the 24 μm data point with the narrow rest-frame 3.3 μm PAH at $z > 7$, while a better fit is achieved with the broad PAH features at rest-frame 6–8 μm. Therefore, the inclusion of 24 μm photometry can directly exclude the deceiving $z > 7$ solution without fine-tuning the fluxes and flux uncertainties from Ling et al. (2024), and is a straightforward remedy for avoiding the erroneous photo-z of COSBO-7 and could prevent similar situations other objects. This demonstrates that long-wavelength MIR photometry can significantly improve the photo-z of DSFGs.

It remains puzzling that the best-fit photo-$z \sim 2.3$ does not agree well with $z_{spec} = 2.625$. In the right panel of Fig. 3, we show the SED fitting at both redshifts. Interestingly, a significant discrepancy is found for F115W, where the F115W measurement from Ling et al. (2024) is clearly above the SED of $z_{spec} = 2.625$. As no strong line is expected in the F115W filter, this discrepancy suggests that the F115W flux is overestimated or that the flux uncertainty is underestimated. Given that this F115W photometry was better fitted by $z > 7$ models (Ling et al. 2024), the F115W measurement is likely problematic, and could also be a reason for the photo-z failure.

4.2. Caution on photo-z

As COSBO-7 is a strongly lensed galaxy with multiwavelength JWST photometry spanning NIR to MIR, it is alarming that the photo-z failed dramatically, undermining the physical parameters relying on it. Given that COSBO-7 is a typical DSFG at $z \sim 2.6$, such photo-z failure could occur in other galaxies. As depicted by the PDF(z) of COSBO-7 from Ling et al. (2024), there are no visible peaks at $z < 5$ from `LePhare` and $z < 4$ from `Bagpipes`; however, the statistically disfavored peak around $z \sim 2.6$ from `EAZY` and `CIGALE` is now proven to be closer to the real solution. This highlights that caution should be exercised when interpreting the output of photo-z codes, and low-z solutions that appear statistically insignificant in the PDF(z) cannot be ruled out.

As demonstrated in Sect. 4.1, it is also remarkable that a subtle adjustment of the F090W upper limit can tremendously impact the robustness of the photo-z. Finally, it is also clear that a combination of photo-z with a single line detection in the mm might not be sufficient for a robust determination of the redshift of DSFGs, especially if the emission line is consistent with multiple solutions. Indeed, this combination entails the danger of providing a deceiving preference for the most exotic but wrong solution. We note that Ling et al. (2024) did highlight uncertainties regarding the $z > 7$ solution and pointed out that low-z solutions cannot be totally ruled out, although their work only shows that high-z solutions are favored.

It is unclear as to whether COSBO-7 is a rare case or similar catastrophic photo-z failures are common among DSFGs. A large sample is required to determine whether these failures are prevalent or even systematic. If such failures were found to be systematic, literature studies relying purely on photo-z and pseudo-spectroscopic redshifts from single line detection would need to be revised.

5. Conclusions

Using ALMA observations, we confirmed that the $z > 7$ DSFG candidate COSBO-7 is, in reality, at $z = 2.625$. Our conclusions are as follows:

1. We detect three lines with a high level of certainty and identify them as CO(3–2), CO(7–6), and [CI](2–1) at $z = 2.625$, thereby robustly confirming the redshift of COSBO-7. This is in tension with the photometric redshift of $z \gtrsim 7.0$ reported by Ling et al. (2024).
2. With the confirmed redshift, we derive physical parameters for COSBO-7 and find it to be a main sequence galaxy with possible optically thick dust.
3. We examined possible explanations for the catastrophic photo-z failure, and attribute it to (1) the likely underestimation of the F090W upper limit and the F115W flux uncertainty; and (2) the lack of photometry at wavelengths beyond 20 μm sampling the PAH features at $z \sim 2.6$.
4. Notably, we recover an almost accurate $z_{phot} \sim 2.3$ by including the MIPS 24 μm photometry without applying further changes with respect to the literature photometry. This provides a straightforward remedy for the erroneous photo-z, and demonstrates the importance of long-wavelength MIR data in supporting photo-z measurements.

This work highlights a common challenge in modeling the SEDs of DSFGs, and provides a cautionary tale regarding the

reliability of photometric redshifts and redshifts that rely on single line detections. Long-wavelength MIR photometry can significantly improve the photo-z quality, and so we encourage the use of MIPS or MIRI 24 μm in SED fitting. However, even with this additional sampling, the photo-z accuracy is still dependent on the sufficient dominance of certain spectral features. As such, detecting multiple lines remains the only way to unambiguously identify the redshifts of DSFGs, and the future Wideband Sensitivity Upgrade of ALMA will turn it into an even more powerful "redshift machine".

Acknowledgements. We thank Haojing Yan, Emanuele Daddi, Jorge Zavala and Ian Smail for helpful discussions in the preparation of this manuscript. We thank Frank Bertoldi for constructive and insightful review of this manuscript. This paper makes use of the following ALMA data: ADS/JAO.ALMA#2023.A.00021, 2022.1.00863, 2021.1.00705.S, and 2016.1.00463.S. ALMA is a partnership of ESO (representing its member states), NSF (USA) and NINS (Japan), together with NRC (Canada), NSTC and ASIAA (Taiwan), and KASI (Republic of Korea), in cooperation with the Republic of Chile. The Joint ALMA Observatory is operated by ESO, AUI/NRAO and NAOJ. SJ acknowledges financial support from the European Union's Horizon Europe research and innovation program under the Marie Skłodowska-Curie grant No. 101060888. JH acknowledges support from the ERC Consolidator Grant 101088676 (VOYAJ). GEM and SJ acknowledge the Villum Fonden research grants 37440 and 13160. The Cosmic Dawn Center (DAWN) is funded by the Danish National Research Foundation under grant DNRF140. APV acknowledges support from the Carlsberg Foundation (grant no CF20-0534).

References

Akins, H. B., Casey, C. M., Allen, N., et al. 2023, ApJ, 956, 61
Aretxaga, I., Wilson, G. W., Aguilar, E., et al. 2011, MNRAS, 415, 3831
Arnouts, S., Cristiani, S., Moscardini, L., et al. 1999, MNRAS, 310, 540
Arrabal Haro, P., Dickinson, M., Finkelstein, S. L., et al. 2023, Nature, 622, 707
Atek, H., Shuntov, M., Furtak, L. J., et al. 2023, MNRAS, 519, 1201
Barrufet, L., Oesch, P. A., Weibel, A., et al. 2023, MNRAS, 522, 449
Bertoldi, F., Carilli, C., Aravena, M., et al. 2007, ApJS, 172, 132
Boone, F., Schaerer, D., Pelló, R., et al. 2011, A&A, 534, A124
Boquien, M., Burgarella, D., Roehlly, Y., et al. 2019, A&A, 622, A103
Brammer, G. B., van Dokkum, P. G., & Coppi, P. 2008, ApJ, 686, 1503
Carnall, A. C., McLure, R. J., Dunlop, J. S., & Davé, R. 2018, MNRAS, 480, 4379
Carniani, S., Hainline, K., D'Eugenio, F., et al. 2024, Nature, 633, 318
Casey, C. M., Kartaltepe, J. S., Drakos, N. E., et al. 2023, ApJ, 954, 31
Casey, C. M., Akins, H. B., Shuntov, M., et al. 2024, ApJ, 965, 98
Chabrier, G. 2003, PASP, 115, 763
Chakraborty, P., Sarkar, A., Wolk, S., et al. 2024, ArXiv e-prints [arXiv:2406.05306]
Chen, C.-C., Liao, C.-L., Smail, I., et al. 2022, ApJ, 929, 159
Cox, P., Neri, R., Berta, S., et al. 2023, A&A, 678, A26
da Cunha, E., Charlot, S., & Elbaz, D. 2008, MNRAS, 388, 1595
da Cunha, E., Walter, F., Smail, I. R., et al. 2015, ApJ, 806, 110
Delvecchio, I., Daddi, E., Sargent, M. T., et al. 2021, A&A, 647, A123
Donnan, C. T., McLeod, D. J., Dunlop, J. S., et al. 2023, MNRAS, 518, 6011
Dudzevičiūtė, U., Smail, I., Swinbank, A. M., et al. 2020, MNRAS, 494, 3828
Dunlop, J. S., Abraham, R. G., Ashby, M. L. N., et al. 2021, PRIMER: Public Release IMaging for Extragalactic Research, JWST Proposal. Cycle 1, ID. 1837
Endsley, R., Stark, D. P., Fan, X., et al. 2022, MNRAS, 512, 4248
Finkelstein, S. L., Bagley, M. B., Arrabal Haro, P., et al. 2022, ApJ, 940, L55
Fudamoto, Y., Oesch, P. A., Schouws, S., et al. 2021, Nature, 597, 489
Geach, J. E., Dunlop, J. S., Halpern, M., et al. 2017, MNRAS, 465, 1789
Gómez-Guijarro, C., Riechers, D. A., Pavesi, R., et al. 2019, ApJ, 872, 117
Harikane, Y., Ouchi, M., Oguri, M., et al. 2023, ApJS, 265, 5
Hygate, A. P. S., Hodge, J. A., da Cunha, E., et al. 2023, MNRAS, 524, 1775
Ilbert, O., Arnouts, S., McCracken, H. J., et al. 2006, A&A, 457, 841
Jiao, Q., Zhao, Y., Lu, N., et al. 2019, ApJ, 880, 133
Jin, S., Daddi, E., Liu, D., et al. 2018, ApJ, 864, 56
Jin, S., Daddi, E., Magdis, G. E., et al. 2019, ApJ, 887, 144
Jin, S., Daddi, E., Magdis, G. E., et al. 2022, A&A, 665, A3
Kokorev, V. I., Magdis, G. E., Davidzon, I., et al. 2021, ApJ, 921, 40
Kriek, M., van Dokkum, P. G., Labbé, I., et al. 2009, ApJ, 700, 221
Ling, C., Sun, B., Cheng, C., et al. 2024, ApJ, 969, L28
Liu, D., Lang, P., Magnelli, B., et al. 2019, ApJS, 244, 40
Magdis, G. E., Daddi, E., Béthermin, M., et al. 2012, ApJ, 760, 6
Magdis, G. E., Rigopoulou, D., Daddi, E., et al. 2017, A&A, 603, A93
Marrone, D. P., Spilker, J. S., Hayward, C. C., et al. 2018, Nature, 553, 51
McMullin, J. P., Waters, B., Schiebel, D., Young, W., & Golap, K. 2007, ASP Conf. Ser., 376, 127
Miettinen, O., Smolčić, V., Novak, M., et al. 2015, A&A, 577, A29
Naidu, R. P., Oesch, P. A., Setton, D. J., et al. 2022, ArXiv e-prints [arXiv:2208.02794]
Neri, R., Cox, P., Omont, A., et al. 2020, A&A, 635, A7
Pearson, J., Serjeant, S., Wang, W.-H., et al. 2024, MNRAS, 527, 12044
Riechers, D. A., Bradford, C. M., Clements, D. L., et al. 2013, Nature, 496, 329
Riechers, D. A., Leung, T. K. D., Ivison, R. J., et al. 2017, ApJ, 850, 1
Riechers, D. A., Boogaard, L. A., Decarli, R., et al. 2020, ApJ, 896, L21
Rizzo, F., Vegetti, S., Fraternali, F., & Di Teodoro, E. 2018, MNRAS, 481, 5606
Rowland, L. E., Hodge, J., Bouwens, R., et al. 2024, ArXiv e-prints [arXiv:2405.06025]
Sargent, M. T., Daddi, E., Béthermin, M., et al. 2014, ApJ, 793, 19
Schinnerer, E., Sargent, M. T., Bondi, M., et al. 2010, ApJS, 188, 384
Schreiber, C., Pannella, M., Leiton, R., et al. 2017, A&A, 599, A134
Schreiber, C., Elbaz, D., Pannella, M., et al. 2018, A&A, 609, A30
Sillassen, N. B., Jin, S., Magdis, G. E., et al. 2024, A&A, 690, A55
Simpson, J. M., Swinbank, A. M., Smail, I., et al. 2014, ApJ, 788, 125
Simpson, J. M., Smail, I., Swinbank, A. M., et al. 2019, ApJ, 880, 43
Simpson, J. M., Smail, I., Dudzevičiūtė, U., et al. 2020, MNRAS, 495, 3409
Smail, I., Dudzevičiūtė, U., Stach, S. M., et al. 2021, MNRAS, 502, 3426
Smolčić, V., Novak, M., Bondi, M., et al. 2017, A&A, 602, A1
Strandet, M. L., Weiss, A., De Breuck, C., et al. 2017, ApJ, 842, L15
Valentino, F., Magdis, G. E., Daddi, E., et al. 2018, ApJ, 869, 27
Vegetti, S., & Koopmans, L. V. E. 2009, MNRAS, 392, 945
Vieira, J. D., Crawford, T. M., Switzer, E. R., et al. 2010, ApJ, 719, 763
Vieira, J. D., Marrone, D. P., Chapman, S. C., et al. 2013, Nature, 495, 344
Walter, F., Decarli, R., Carilli, C., et al. 2012, Nature, 486, 233
Wang, T., Schreiber, C., Elbaz, D., et al. 2019, Nature, 572, 211
Wardlow, J. L., Smail, I., Coppin, K. E. K., et al. 2011, MNRAS, 415, 1479
Witstok, J., Smit, R., Maiolino, R., et al. 2022, MNRAS, 515, 1751
Zavala, J. A., Montaña, A., Hughes, D. H., et al. 2018, Nat. Astron., 2, 56
Zavala, J. A., Buat, V., Casey, C. M., et al. 2023, ApJ, 943, L9

[1] Cosmic Dawn Center (DAWN), Denmark
[2] DTU Space, Technical University of Denmark, Elektrovej 327, DK-2800 Kgs. Lyngby, Denmark
[3] Leiden Observatory, Leiden University, P.O. Box 9513, 2300 RA Leiden, The Netherlands
[4] Niels Bohr Institute, University of Copenhagen, Jagtvej 128, DK-2200 Copenhagen, Denmark
[5] Kapteyn Astronomical Institute, University of Groningen, 9700, AV Groningen, The Netherlands
[6] The University of Texas at Austin, 2515 Speedway Blvd Stop C1400, Austin, TX 78712, USA
[7] Space Telescope Science Institute, 3700 San Martin Drive, Baltimore, MD 21218, USA
[8] European Southern Observatory (ESO), Karl-Schwarzschild-Strasse 2, Garching 85748, Germany
[9] Université Paris-Saclay, Université Paris Cité, CEA, CNRS, AIM, 91191 Gif-sur-Yvette, France
[10] Instituto de Física, Pontificia Universidad Católica de Valparaíso, Casilla 4059, Valparaíso, Chile
[11] Caltech/IPAC, MS 314-6, 1200 E. California Blvd, Pasadena, CA 91125, USA
[12] Laboratory for Multiwavelength Astrophysics, School of Physics and Astronomy, Rochester Institute of Technology, 84 Lomb Memorial Drive, Rochester, NY 14623, USA
[13] Max-Planck-Institut für Astronomie, Königstuhl 17, 69117 Heidelberg, Germany
[14] Hiroshima Astrophysical Science Center, Hiroshima University, 1-3-1 Kagamiyama, Higashi-Hiroshima, Hiroshima 739-8526, Japan
[15] National Astronomical Observatory of Japan, 2-21-1, Osawa, Mitaka, Tokyo, Japan
[16] Purple Mountain Observatory, Chinese Academy of Sciences, 10 Yuanhua Road, Nanjing 210023, China
[17] University of Bologna, Department of Physics and Astronomy (DIFA), Via Gobetti 93/2, I-40129 Bologna, Italy
[18] INAF – Osservatorio di Astrofisica e Scienza dello Spazio, Via Gobetti 93/3, 40129 Bologna, Italy

Appendix A: Supporting material

Table A.1. MIR to radio photometry

Facility	Band	Flux/mJy
Spitzer/MIPS	24 μm	0.188 ± 0.046
Herschel/PACS	100 μm	0.01 ± 1.57
Herschel/PACS	160 μm	9.72 ± 2.52
Herschel/SPIRE	250 μm	18.81 ± 1.79
Herschel/SPIRE	350 μm	28.60 ± 2.89
Herschel/SPIRE	500 μm	24.66 ± 2.06
SCUBA-2	850 μm	9.71 ± 0.67
ALMA*	870 μm	10.45 ± 0.60
AzTEC	1.1 mm	5.55 ± 1.29
MAMBO	1.2 mm	4.84 ± 0.69
ALMA	237.5 GHz	3.65 ± 0.47
ALMA	224.8 GHz	3.41 ± 0.41
ALMA	145 GHz	0.62 ± 0.07
ALMA	100 GHz	0.071 ± 0.016
VLA	3 GHz	$(28.6 \pm 2.8) \times 10^{-3}$
VLA	1.4 GHz	$(91.4 \pm 10.2) \times 10^{-3}$

Notes: * From A3COSMOS catalog (Liu et al. 2019).

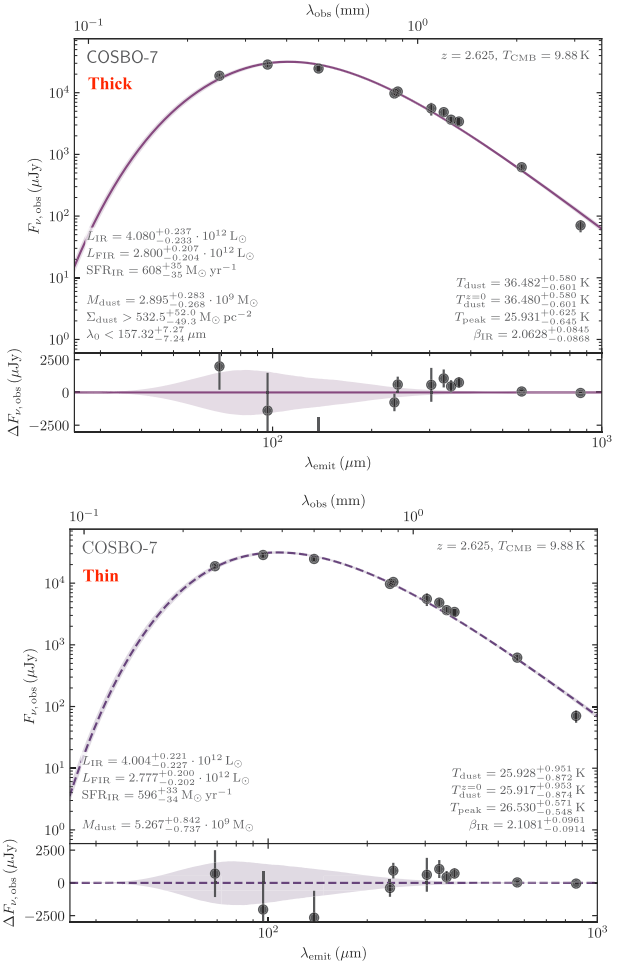

Fig. A.1. FIR SEDs in optically thick (upper) and thin (bottom) dust models, fitted with `Mercurius` (Witstok et al. 2022).

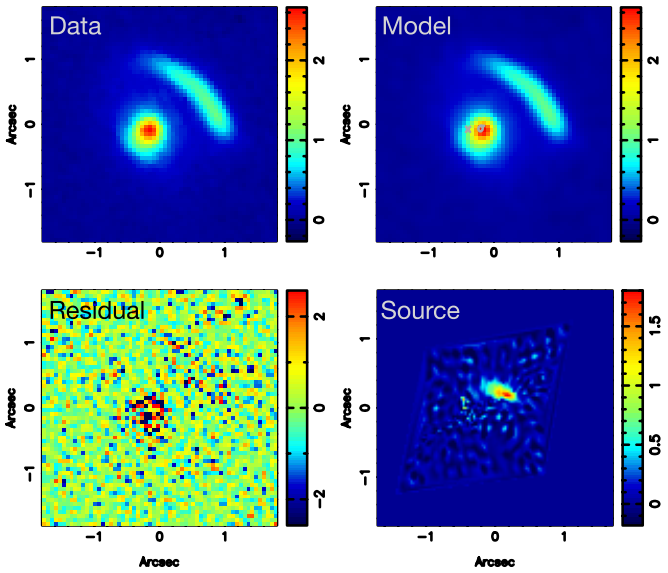

Fig. A.2. The lens model in the MIRI F770W band. The data is well modeled with a magnification factor $\mu = 3.6^{+2.0}_{-0.9}$ using the method **from** Rizzo et al. (2018). We show the data, model, residual and reconstructed source image, respectively.